

Gold

Mild Homogeneous Synthesis of Gold Nanoparticles through the Epoxide Route: Kinetics, Mechanisms, and Related One-Pot Composites

V́ctor Oestreicher,^{*,[a, b, e]} Cristián Huck-Iriart,^[c] Galo Soler-Illia,^[a] Paula C. Angelomé,^[b] and Matías Jobbágy^{*,[d]}

Dedicated to Professor Enrique San Román

Abstract: A new one-pot homogeneous methodology at room temperature to obtain Au nanoparticles (AuNP) on the basis of the epoxide route is presented. The proposed method takes advantage of the homogenous generation of OH⁻ moieties driven by epoxide ring-opening, mediated by chloride nucleophilic attack. Once reached alkaline conditions, the reducing medium allows the quantitative formation of AuNP under well-defined kinetic control. A stabilizing agent, such as polyvinylpyrrolidone (PVP) or cetyltrimethylammonium chloride (CTAC), is required to maintain the AuNP stable. Meanwhile their presence dramatically affects the reduction kinetics and pathway, as demonstrated by the evolution of the UV/Vis spectra, small-angle X-ray scattering

(SAXS) patterns, and pH value along the reaction. In the presence of PVP nanogold spheroids are obtained following a similar reduction mechanism as that observed for control experiments in the absence of PVP. However, if CTAC is employed a stable complex with Au^{III} is formed, leading to a different reaction pathway and resulting in ellipsoidal-like shaped AuNP. Moreover, the proposed methodology allows stabilize the growing AuNP, by coupling their formation with nonalkoxidic sol-gel reactions, leading to nanocomposite gels with embedded metallic nanoparticles. The epoxide route thus offers a versatile scenario for the one-pot preparation of new metal nanoparticles-inorganic/hybrid matrices nanocomposites with valuable optical properties.

Introduction

Gold nanoparticles (AuNP) are among the most studied noble metal nanoparticles because of their key role in fundamental

and applied nanoscience.^[1] Several morphologies and sizes could be obtained nowadays, such as spheres, rods, triangles, bipyramids, among others.^[2,3,4] This wide variety of AuNP with well-controlled sizes and shapes was exploited for the production of new optical sensors,^[5,6] sensors based on surface-enhanced Raman spectroscopy,^[7,8] more efficient catalysts,^[9,10,11,12] and for innovative medical^[13,14] and biological applications.^[15,16] Depending on the chosen applications, the nanoparticles can be used directly in solution, forming arrays onto surfaces^[17] or embedded in inorganic or polymeric matrices, in nanocomposites.^[18,19,10,12] The reported methods to obtain such nanoparticles typically involve the direct mixture of the reagents and can be divided into two families: one-step synthesis or seed-mediated approaches.^[2] While the former are inherently easier to implement, the latter offer a more accurate textural control over the final nanoparticles, achieving sophisticated morphologies. Nowadays, much effort is focused on improving the performance of one-pot routes, elucidating the role of the most relevant and eventually hidden experimental variables. Perhaps the most popular one-step approach is the Turkevich method,^[20] which consists in adding a reducing agent (sodium citrate), adjusted at a suitable pH value, to a boiling tetrachloroauric acid solution. In this case, in the starting reagent's mixture Au^{III} ions are instantly exposed to a quantitative driving force for their reduction. Spheroidal AuNP with a diameter around 15 nm are obtained by this means. Even this relatively

[a] Dr. V. Oestreicher, Prof. Dr. G. Soler-Illia
Instituto de Nanosistemas, UNSAM, CONICET
25 de mayo 1021, San Martín, 1650 Buenos Aires (Argentina)
E-mail: victor.oestreicher@uv.es

[b] Dr. V. Oestreicher, Dr. P. C. Angelomé
Gerencia Química & Instituto de Nanociencia y Nanotecnología
Centro Atómico Constituyentes
Comisión Nacional de Energía Atómica, CONICET
Av. Gral. Paz 1499, San Martín B1650KNA Buenos Aires (Argentina)

[c] Dr. C. Huck-Iriart
Escuela de Ciencia y Tecnología, UNSAM, CONICET
25 de mayo 1650, San Martín 1650, Buenos Aires (Argentina)

[d] Prof. Dr. M. Jobbágy
Departamento de Química Inorgánica
Analítica y Química Física/INQUIMAE
Facultad de Ciencias Exactas y Naturales, Universidad de Buenos Aires
Ciudad Universitaria, Pab. II, Buenos Aires C1428EHA (Argentina)
E-mail: jobbag@qi.fcen.uba.ar

[e] Dr. V. Oestreicher
Current address: Instituto de Ciencia Molecular (ICMol)
Universidad de Valencia, Catedrático José Betrán 2
46980, Paterna, Valencia (Spain)

Supporting information and the ORCID identification number(s) for the author(s) of this article can be found under:
<https://doi.org/10.1002/chem.201905335>

simple synthesis, which has been tested for more than 60 years, is still being revisited in the recent literature, with the objective of controlling size reproducibility and monodispersity of the resulting AuNP.^[21,22] For example, Ojea-Jiménez et al.^[23] have demonstrated that the mixing sequence of the reagents has an effect on the AuNP size and morphology. Also, Schulz et al.^[24] demonstrated that there is an optimal pH value that gives rise to uniform and monodisperse AuNP. In the same sense, Kettermann et al.^[25] studied the Turkevich method in great detail alerting about the influence of the resulting pH of the solution on the size and polydispersion of the obtained AuNP. In recent years, milder reducing agents such as alcohols and polyols gained increasing attention, because they offer a proper reactivity in aqueous media, defining a highly eco-friendly synthesis.^[26,27,28,29,30] However, the inherently inconvenient scenario, related to the mixing sequence of the reagents and pH optimization, still remains.^[31]

Most of these inherent drawbacks related to adding and mixing solutions that are dramatically far from chemical equilibrium, can be solved by employing homogeneous synthesis methods. In those ones, the chemical driving force for particle formation is activated after mixing the reagents, typically by temperature increment or the in situ generation of one of the reagents. This approach ensures that both the nucleation and growth of the particles take place in the absence of any compositional inhomogeneity in the solution.

In this context, the in situ alkalization of a solution containing Au^{III} precursors in the presence of a reducing agent, which can only effectively react under alkaline conditions, can fulfil the requirements for a one-pot synthesis on a homogeneous basis.

In recent years, the epoxide route has demonstrated a great versatility to drive the homogenous alkalization of acidic solutions at room temperature. Nucleophilic attack over epoxides, typically driven by chloride,^[32] is able to drive the precipitation of several inorganic materials with an exquisite textural control,^[33,34] including metal (hydro)oxides,^[35] layered basic salts,^[36,37] layered double hydroxides,^[32,38,39] silicates,^[40] phosphates,^[41] and, more recently, hybrid layered structures and metal organic frameworks.^[42] In all the cases a one-pot approach under room temperature conditions is used. In parallel, coupled with the alkalization process, this in situ method releases diols to the media, which result from the partial hydrolysis of the epoxide. Taking into account the mild and controllable release of diol and hydroxide to the reaction medium, the epoxide route can potentially drive metallic gold formation, on the basis of an irreversible redox process.

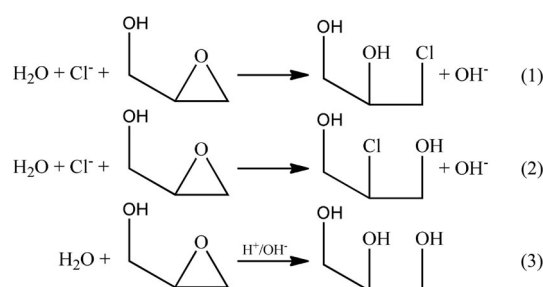
The present work introduces the homogeneous reduction of HAuCl₄ into metallic AuNP through the epoxide route for the very first time. The homogeneous growth mechanism is comprehensively studied by means of in situ UV/Vis spectroscopy, small-angle X-ray scattering (SAXS) and pH evolution characterization, alerting about the non-innocent role of the stabilizing agent in the chemical speciation of Au^{III} and its reactivity. In addition, we present a particular application in which the reduction process is sequentially coupled with a non-alkoxidic sol-gel process, leading to nanocomposites (AuNP in inorganic

hydrogels) of high optical quality on a one-pot basis. This work paves the way towards the generation of a wide variety of AuNP and composites by one-pot homogenous methods at room temperature. Moreover, it demonstrates the feasibility of using such methods to perform careful physicochemical characterization of the AuNP formation process.

Results and Discussion

Synthesis feasibility

The alkalization method based on the epoxide route consists in the nucleophilic attack over an electrophilic carbon belonging to the epoxide ring.^[32] This reaction, typically carried out by chloride anions added as KCl, results in the epoxide ring-opening of glycidol (or Gly) in the present case, and chlorohydrin formation (see Scheme 1, reactions 1 and 2). Nevertheless, the aqueous medium itself is able to decompose Gly through a hydrolytic attack, which results in the formation of glycerol (see Scheme 1, reaction 3). This side reaction, which does not contribute to the net alkalization, is favored either in acid or alkaline media.



Scheme 1. Ring-rupture reaction of glycidol in aqueous media: chloride attack with chlorohydrin formation and net alkalization (reactions 1 and 2) or epoxide hydrolysis (acid- or base-catalyzed glycerol formation, reaction 3).

In order to evaluate the feasibility of the epoxide route to drive Au^{III} reduction, HAuCl₄, KCl, and the main reducing agent, glycerol, were mixed at room temperature (see Experimental Section), on the basis of typical AuNP synthesis procedures through polyol reduction. No signs of reduction were observed when HAuCl₄ (acid precursor) and KCl were mixed in the presence of glycerol; alkaline media (KOH) in the absence of glycerol gave similar results. Quantitative reduction took place once this solution was mixed under alkaline conditions, which confirms the inherent reducing ability of polyols at room temperature, once pH is raised to the proper value.^[26,27,28,29,30]

Once the potential ability of Gly to drive the homogenous reduction of Au^{III} was established, the experimental conditions were screened in order to ensure the quantitative formation of metallic nanoparticles, on the basis of the inherent reactivity of these reagents.^[32] When Gly (responsible of the alkalization reaction and polyol generation, see Scheme 1) was added, the initial HAuCl₄ yellow solution, containing chloride anions, turned colorless and then reddish, indicating quantitative re-

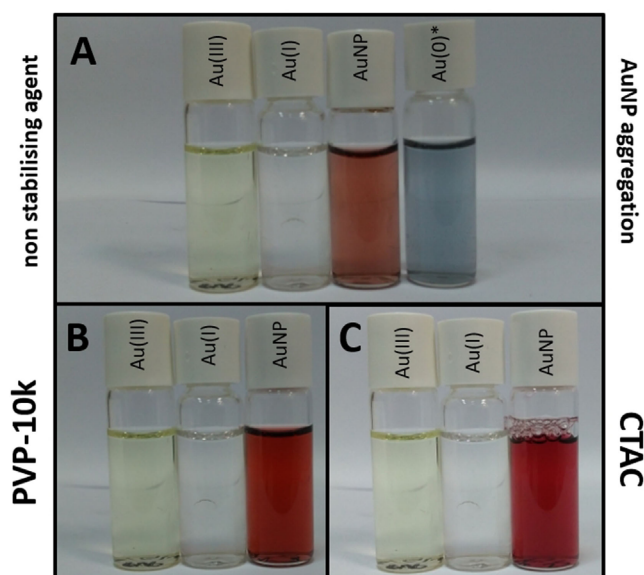


Figure 1. Images of representative samples belonging to the different states reached along the reaction by employing initial concentrations of $[\text{HAuCl}_4] = 0.5 \text{ mM}$, $[\text{Cl}^-] = 100 \text{ mM}$, $[\text{Gly}] = 2500 \text{ mM}$ A) without stabilizing agent and with B) $[\text{PVP-10k}] = 0.11 \text{ mM}$ (B) or C) $[\text{CTAC}] = 10 \text{ mM}$ at 25°C .

duction of Au^{III} to Au^{I} subsequently followed by Au nanoparticle formation. Nevertheless, the obtained nanoparticles tended to aggregate and precipitate along their growth, as presented in Figure 1 A; UV/Vis spectra also confirmed this naked-eye observation (see Figure S1). This result suggests that products of the Gly ring-opening, glycerol and both chlorohydrin isomers, or their resulting oxidized forms, are not effective stabilizing agents, because AuNP tend to agglomerate, which is due the high ionic strength given by at least 100 mM of K^+ . Aiming at improving the epoxide route as a synthetic method, already proved by the sequential reduction of $\text{Au}^{\text{III}} \rightarrow \text{Au}^{\text{I}} \rightarrow \text{Au}^{\text{0}}$, a stabilizing agent must be used in order to avoid aggregation. Polyvinylpyrrolidone, $M_w = 10000 \text{ g mol}^{-1}$ (PVP-10k), and cetyltrimethylammonium chloride (CTAC) were chosen as polymeric and cationic stabilizing agents, respectively. In these samples, Gly was added to solutions containing HAuCl_4 , KCl , and PVP-10k or CTAC at room temperature; none of these additives affected the alkalization rate of the chloride–Gly reaction (see Figure S2). An analogous quantitative reduction sequence was observed while reddish AuNP suspensions that remain stable for months were obtained (Figure 1 B and C).

TEM inspection of the stabilized AuNP is presented in Figure 2. Morphological characterization by TEM performed over more than 100 nanoparticles of both samples allowed to confirm the formation of spheroidal nanoparticles with diameters of 10 ± 2 and $14 \pm 3 \text{ nm}$ for PVP-10k and CTAC, respectively. These experiments demonstrate the feasibility of the proposed synthetic methodology to obtain spheroidal AuNP, exclusively, in a homogeneous one-pot reaction at room temperature.

Kinetics of Au^{III} reduction and the effect of stabilizing agents on the growth mechanism

In order to perform a further inspection of the main parameters that govern the alkalization reaction, the variation of both chloride and glycidol concentrations could be explored. Chloride concentration modulates both the gold reduction potential (see Figure S3) and the alkalization (reactions 1 and 2, Scheme 1) versus hydrolysis (reaction 3, Scheme 1) rates.^[32] In the present approach, in order to realize a simplified kinetics screening, only the glycidol concentration was explored as the experimental parameter to regulate the reaction rate. A set of experiments screening initial glycidol concentrations from 250 to 5000 mM were carried out in the presence of each of the stabilizing agents. Under all evaluated conditions stable AuNP were obtained. Reaction time decreases when glycidol concentration increases as expected according to the alkalization rate [Eq. 1]:

$$v_{\text{OH}^-} = \frac{d[\text{OH}^-]}{dt} = k[\text{Cl}^-][\text{Gly}] \quad (1)$$

Reaction completion can be tuned from 30 minutes to one day and from 10 minutes to a couple of hours when CTAC or PVP-10k are used as stabilizing agents, respectively. For each condition, experiments performed by using CTAC were always faster than those with PVP-10k. Figure S4 depicts UV/Vis spectra of the prepared samples, with their localized surface plasmon resonance (LSPR) band position. A clear trend for the PVP-10k experiment is observed. The LSPR band position shifts from about 530 to about 510 nm with glycidol concentration increment. However, for CTAC experiments, the LSPR band position remains practically invariant around $523 \pm 1 \text{ nm}$ under the same scenario. In all the experiments, the absorbance at 400 nm reaches the expected value of 1.20 ± 0.05 , which indicates a quantitative reduction of Au^{III} into metallic nanoparti-

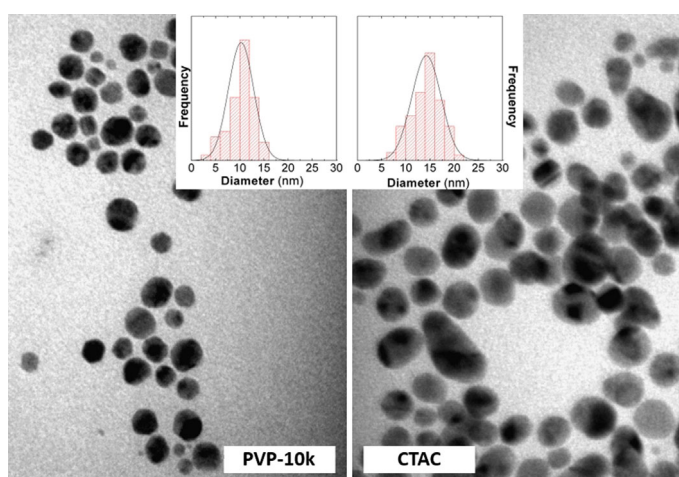


Figure 2. TEM images of AuNP obtained by employing initial concentrations of $[\text{HAuCl}_4] = 0.5 \text{ mM}$, $[\text{Cl}^-] = 100 \text{ mM}$, $[\text{Gly}] = 2500 \text{ mM}$, and $[\text{PVP-10k}] = 0.11 \text{ mM}$ (left); or $[\text{CTAC}] = 10 \text{ mM}$ (right) at 25°C ; scale bar represents 50 nm for both images. Inset: size distribution estimated over more than 100 nanoparticles.

cles.^[43] These experiments demonstrate that AuNP can be obtained under a wide range of experimental conditions, and their characteristics depend on both glycidol concentration and the chosen stabilizing agent. In order to understand the reduction sequence (already observed by the naked eye, Figure 1) and how the alkalization method controls the reduction process, detailed kinetic studies were performed under a given glycidol-to-Au^{III} ratio. Figure 3 depicts the characteristic evolution of the UV/Vis spectra recorded during the reaction in the presence of each one of the stabilizing agents, PVP-10k

and CTAC; a control experiment in the absence of stabilizer is also presented. The inspection of the bands around 275–375 nm gives information about the presence of Au^{III} complexes,^[44] whereas the absorption bands in the 375–825 nm region give information about the LSPR band of AuNP, the position of which is related to their shape and size.^[45]

While the reaction proceeds and pH increases, a blueshift is observed at the maximum position of Au^{III} in PVP-10k solution; this behavior was also found in solutions containing HAuCl₄ and KCl without stabilizing agents (control). Such continuous shift is related to the substitution of Cl⁻ by OH⁻ in Au(OH)_xCl_{4-x}⁻ moieties, with 0 ≤ x ≤ 4 (see Figure S5), as was reported for titration experiments in which total ligand exchange was achieved.^[46] The rate of decay of Au^{III} moieties and the subsequent growth of AuNP are practically identical in the presence or absence of PVP (see Figure S6). Once approximately 20% of gold has been reduced to the metallic state, dramatic differences between the PVP sample and the control are observed. While the former develops a constant rate growth the latter exhibits an accelerated profile until 60% of reduction. At this value, quantitative aggregation and flocculation takes place with the subsequent absorbance decay.

Marked differences are observed for both Au^{III} and AuNP regions when alkalization develops in the presence of CTAC. First, a redshift of about 8 nm for the maximum position of Au^{III} is registered for the initial solution containing CTAC. This suggests that the complex between Au^{III} and CTAC (from here Au^{III}-CTAC) is present under these experimental conditions.^[47] However, the maximum position of the Au^{III}-CTAC complex remains practically invariant during its consumption, which shows a higher stability of this complex/moieties over OH⁻ substitution. Although experimental conditions remain constant, and only changes in the nature of stabilizing agent were induced, a clear change in the AuNP growth mechanism results. Looking at the 375–825 nm region, a continuous redshift of the LSPR maximum during AuNP growth can be observed when PVP-10k is used, which is in good agreement with a process that involves the nucleation of nanospheres that increase their size along the reaction. However, when CTAC is used, the behavior is essentially different: a blueshift is observed, matching with a narrowing in the LSPR band. These inherent differences are compiled in Figure S7, which presents the mentioned shifts in the maximum position of Au(OH)_xCl_{4-x}⁻, Au^{III}-CTAC absorption band, and position of the LSPR band of AuNP as a function of reaction time. Beyond the inherent differences between their growth mechanisms, both reactions are completed in terms of Au^{III} consumption, and the obtained AuNP present highly symmetric and narrow LSPR bands with maxima around 518 and 523 nm for PVP-10 K and CTAC, respectively. Even so, the kinetic growth of AuNP is essentially different, around 2–3 times faster when CTAC is employed.

In the search of a detailed morphological characterization of these different growth scenarios, SAXS patterns were recorded during the reaction, in order to model the AuNP size and shape evolution. In this point, it is important to highlight that, because of the strict control in the reaction rate given by the homogeneous alkalization, several SAXS patterns can be

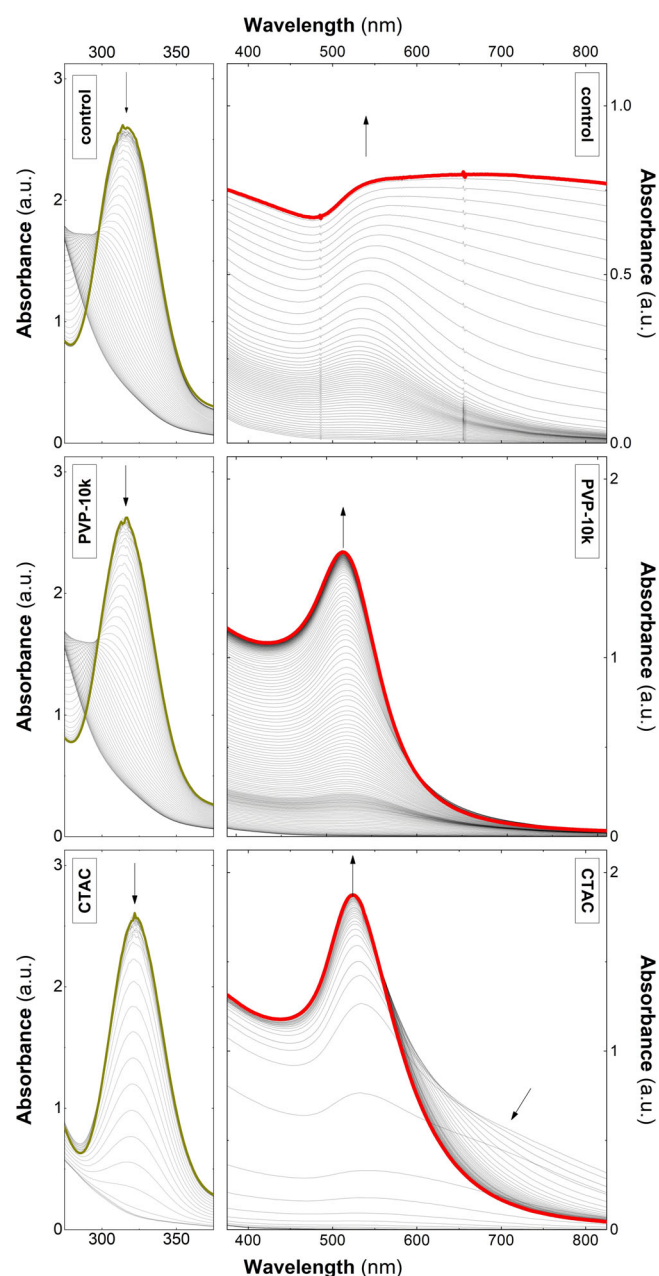


Figure 3. UV/Vis spectra as a function of reaction time (0 to 300 min) for gold reduction mediated by glycidol at 25 °C. The samples were prepared by employing initial concentrations of [HAuCl₄]=0.5 mM, [Cl⁻]=100 mM, [Gly]=2500 mM (control experiment, upper panel) and [PVP-10k]=0.11 mM (central panel) or [CTAC]=10 mM (bottom panel). Arrows indicate the time evolution.

easily obtained, allowing a proper in situ isothermal study of the growth kinetics.^[48,49] A set of SAXS curves obtained at representative times for PVP-10k and CTAC samples are presented in Figure 4. On the basis of the TEM size distribution analysis that showed monomodal histograms for both systems, a non-

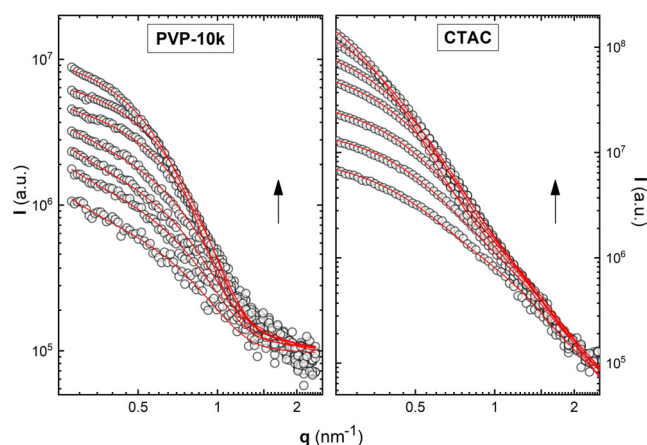


Figure 4. Evolution of SAXS patterns with time (0 to 300 min) and its fitting (red lines) for solutions prepared by employing initial concentrations of $[\text{HAuCl}_4] = 0.5 \text{ mM}$, $[\text{Cl}^-] = 100 \text{ mM}$, $[\text{Gly}] = 2500 \text{ mM}$, and $[\text{PVP 10k}] = 0.11 \text{ mM}$ (left) or $[\text{CTAC}] = 10 \text{ mM}$ (right) at 25°C . Arrows indicate time evolution.

interactive polydisperse ellipsoid of revolution nanoparticle model^[50] was chosen. This model takes into account the anisotropic particle shape and allows performing a proper fitting of each individual pattern (see Appendix in the Supporting Information). In this particular case, a morphology parameter (ϵ) that accounts for the aspect ratio between the equatorial and axial diameters was defined. For the number size distribution, a nonsymmetric Schulz–Zimm^[51] normalized distribution was used, which allows the inclusion of a polydispersity function with a variance (σ) around a size average diameter (D).^[52] In the case of the CTAC system, the specific contribution of the micelles was taken into account in the analysis (see Figure SA1).

For the PVP-10k sample, the average diameter after three hours of reaction results in 8 nm with a 2 nm size distribution variance (see Table 1). PVP-10k-stabilized AuNP can be modeled as spherical objects ($\epsilon \sim 1$) with a diameter that slightly increases after first detection; LSPR band position measurements support this observation. In the case of the CTAC

Table 1. Size parameters obtained from SAXS fitting. $D_{av,N}$ corresponds to the ellipsoid's average equatorial diameter, σ to the Schulz–Zimm variance for number (N) or volume (V) size distribution function, and ϵ to the aspect parameter defined as the ratio between the equatorial and axial diameter.

Stabilizing agent	$D_{av,N}$ [nm]	σ_N	ϵ	$D_{av,V}$ [nm]	σ_V
PVP-10k	6.2 ± 0.1	1.2	0.98 ± 0.03	8.0 ± 0.1	1.6
CTAC	13.3 ± 0.1	3.9	0.73 ± 0.01	16.6 ± 0.1	4.9

sample, the best fit of the SAXS patterns is obtained when an oblate ellipsoid of revolution is assumed ($\epsilon < 1$). The growth curve shows that during the initial stages AuNP present a highly anisotropic aspect ratio of about 0.45 until they reach the maximum size/volume. Close to the end of this first 20 minutes-long step of reduction and growth, the nanoparticles develop a maturation process and after 60 minutes the anisotropic aspect ratio increases its value to 0.73.

It is important to remark that, for both families of final particles, diameters obtained by SAXS pattern modeling are in close agreement with TEM observations. However, spherical and spheroidal particles with these diameters cannot be distinguished by conventional TEM measurements and/or the maximum position in UV/Vis spectra. SAXS analysis supports the observation of other techniques about the influence of the two stabilizing agents during the nanoparticle's nucleation and growth. Moreover, the blueshift observed in UV/Vis spectra after nucleation for CTAC-stabilized samples could be attributed to the nucleation of highly anisotropic nanoparticles ($\epsilon \sim 0.45$), which evolve later into more symmetrical spheroids along the growth process ($\epsilon \sim 0.73$). Table 1 compiles the model's parameter values obtained by a nonlinear square fit of the experimental SAXS patterns for an ex situ experiment performed after three hours of reaction. The values obtained from the volume-size distribution are in accordance with TEM size histograms, because of the stronger incidence of the larger particles on the scattered intensity. All reported values correspond with the volume-size distribution.

The pH evolution was also assessed in order to further understand the reaction steps. Figure 5 compiles this information along with the rate of Au^{III} consumption and reduction into metallic form (AuNP growth) estimated from UV/Vis spectra analysis, and diameter evolution obtained by SAXS fitting. For both CTAC and PVP-10k experiments, as soon as the reaction between chloride and Gly takes place, the pH increases from the acidic conditions given by HAuCl_4 up to the most alkaline conditions that the present method typically reaches, close to a value of 11.^[32]

The reduction in the presence of PVP takes place with a monotonous increment of pH; nucleation of metallic gold takes place at a pH value of 10.0. No pH drops were observed along the nucleation and growth of the metallic phase; having in mind that Au^{III} does not form any complex with PVP-10k, the gold complexes distribution, $\text{Au}(\text{OH})_x\text{Cl}_{4-x}^-$, will be modulated by pH exclusively. Then, highly hydroxylated Au^{III} species prevail, proving the necessary OH equivalents (one per electron) to drive the redox process (see Scheme S1). When Au^{III} is reduced in the presence of CTAC, the pH profile presents abrupt changes in its shape. The first deceleration of pH around 9.0 is coincident with the sudden and massive absorption decay of the initially prevalent Au^{III} -CTAC complex, to give rise to an intermediate moiety. Once a pH value of about 9.5 is reached, the OH^- consumption of this first step ends and the pH curve's slope increases. At a pH value of about 10.2, a sudden pH drop overlaps with the formation of AuNP, in agreement with UV/Vis and SAXS inspection, which suggests the occurrence of a nucleation overshoot. In this moment, the AuNP di-

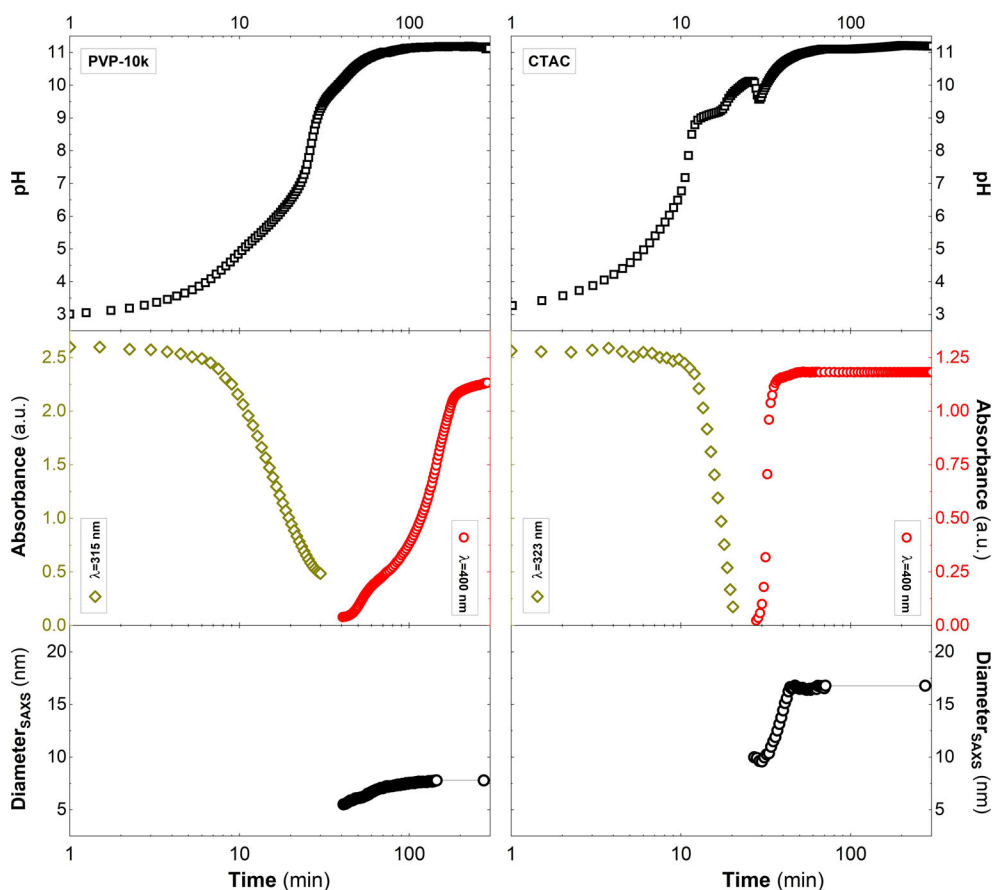


Figure 5. Evolution of pH (upper panel); Au^{III} and Au⁰ UV/Vis traces (central panel); and diameter from SAXS analysis (lower panel) of AuNP employing PVP-10k (left) and CTAC (right). The samples were prepared by employing initial concentrations of [HAuCl₄] = 0.5 mM, [Cl⁻] = 100 mM, [PVP-10k] = 0.11 mM (left), [CTAC] = 10 mM (right), and [Gly] = 2500 mM at 25 °C.

ameter is about half of the final one, which is reached some minutes afterwards. This second marked acidification can be interpreted in terms of sudden consumption of hydroxyl groups required for the oxidation of alcohol groups to aldehydes and/or acids (see Scheme S1). The differences in pH values at which the reaction takes place when comparing with CTAC experiments, alert about modification in the gold species' thermodynamic stability mediated by Au^{III}-CTAC complex formation. When both CTAC and PVP experiments were repeated by employing a lower initial concentration of glycidol (1000 mM), identical pH profiles were observed, which indicates the occurrence of a similar sequence of chemical events or reduction mechanism (see Figure S8–S10); for each system, the overall alkalization/reduction rates were proportionally reduced, according to Equation (1).

In summary, by means of a comprehensive characterization, it was demonstrated that two different mechanisms are involved in the AuNP formation mediated by the epoxide route, depending on the nature of the employed stabilizing agent. This study was possible thanks to the fact that the epoxide decomposition is homogeneous and progressively generates the ideal medium for Au^{III} reduction, along a time scale fully compatible with the most commonly employed techniques in kinetic measurements.

Kinetics of Au^{III} reduction in a sol–gel transition scenario and hydrogel stabilization; towards composites by a one-pot approach

In addition to the explored strategies to stabilize the AuNP, a complementary approach was evaluated, by taking advantage of the mild alkalization conditions employed herein including sol–gel transitions. In principle, the AuNP formation can be combined with other pH-driven chemical transformations; in particular, hydrogels are able to physically trap nanoparticles preventing their aggregation/decantation. By coupling reduction and gelation, composite materials can be prepared through a one-pot approach. In this sense, there is a wide pH window before gold reduction/agglomeration takes place, along which several inorganic matrices such as Zr^{IV},^[53] Al^{III},^[54] or Si^{IV}^[40] based hydrogels may be formed and consolidated, driven by the epoxide route alkalization. Because these phases nucleate and quantitatively grow under relatively acidic conditions, their formation can eventually take place before or along gold reduction, allowing the growth of a composite either in a sequential or simultaneous fashion. In order to illustrate this concept, a set of Al^{III}-based hydrogels were prepared in the presence of increasing concentrations of HAuCl₄, without adding any soluble stabilizing agent. To this aim, both the solvent and the epoxide concentration were modified accord-

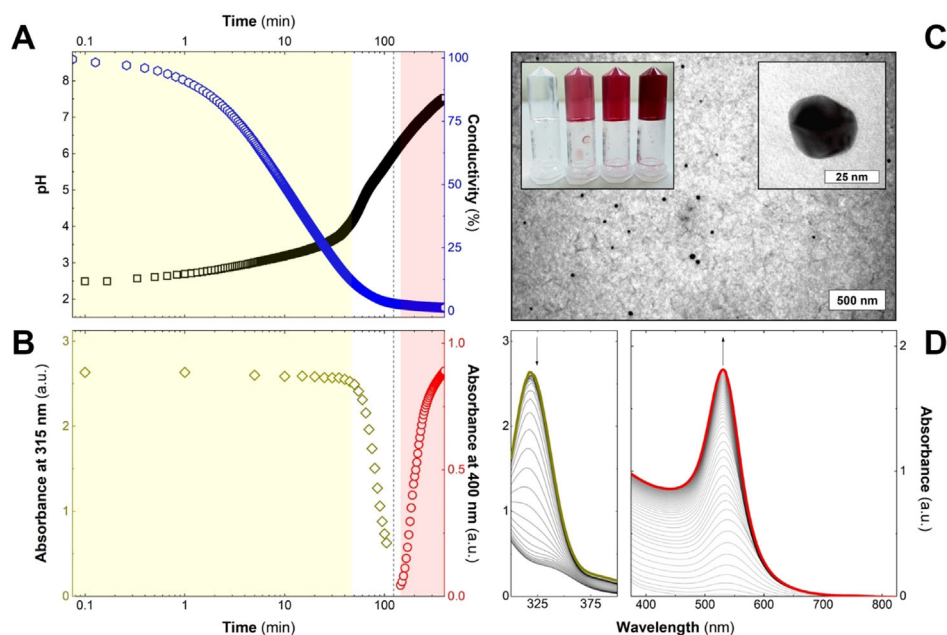


Figure 6. A) Evolution of pH, conductivity, and absorbance (at 315 and 400 nm) for glycerol/water solutions (50% in volume) containing initial concentrations of $[\text{HAuCl}_4] = 0.5 \text{ mM}$, $[\text{AlCl}_3] = 500 \text{ mM}$, and $[\text{Gly}] = 4400 \text{ mM}$ at 25°C . B) Absorbance values recorded at 315 and 400 nm are used to follow the overall consumption of $\text{Au}(\text{OH})_x\text{Cl}_{4-x}^-$ complexes (yellow zone) and AuNP formation (red zone), respectively; dashed line denotes the gelation time. C) Digital image of the resulting $\text{Al}(\text{OH})_3$ hydrogels hosting the grown Au nanoparticles prepared with $[\text{HAuCl}_4] = 0, 0.25, 0.50, \text{ or } 1.0 \text{ mM}$; TEM image of the composite sample with $[\text{HAuCl}_4] = 0.5 \text{ mM}$ aged for 1000 min. D) UV/Vis spectra of the hydrogel as a function of reaction time ($t = 0 \text{ min}$ in yellow, $t = 1000 \text{ min}$ in red); arrows indicate the time evolution.

ing to our previous development of high optical quality hydrogels.^[53] Figure 6 depicts the evolution of pH and conductivity as well as the main UV/Vis absorption signals belonging to the starting Au^{III} precursors and the resultant AuNP. Because the most important contribution to the overall conductivity of the starting solution comes from the AlCl_3 , the conductivity decay offers a robust indication of the extent of hydroxylation/gelation of $\text{Al}(\text{OH})_3$ that drives the sol–gel transition. Between 1 and 30 min, a noticeable drop in the conductivity coexists with an alkalization plateau centered at a pH value of 3.0, governed by the hydroxylation of Al^{III} moieties. Along this step, the sol–gel transition takes place while the concentration of Au^{III} soluble precursors remains almost unaltered. Subsequently, once Al^{III} is quantitatively consumed, evidenced by a conductivity decay of almost 90%, pH rises at a faster rate and when a value of 6 is reached, nucleation of gold takes place and quantitative reduction is observed. The decrease of the nucleation pH can be interpreted in terms of a more reducing medium employed herein (because of the higher initial Gly concentration) and/or the eventual role of $\text{Al}(\text{OH})_3$ surface favoring a heterogenous nucleation process. UV/Vis spectra evidenced an increase in the intensity of the LSPR band, centered at 530 nm, denoting a similar growth mechanism as observed in the control experiment in the absence of stabilizing agents (see Figure 3). In this case, the lack of specific shifts associated with nanoparticle aggregation, even for the highest Au^{III} concentration tested, suggests the growth of AuNP within the microstructure of the hydrogel, avoiding their migration. Beyond these mechanistic aspects, it is worth to mention that the $\text{Al}(\text{OH})_3$ hydrogel has a neglectable contribution to the absorp-

tion signal along the whole sol–gel and reduction process, as was observed before for related systems, such as nano- ZrO_2 hydrogels.^[53] TEM images (Figure 6c) demonstrate that the obtained AuNP are isolated and present a spheroidal shape with an average diameter of 20 nm. This set of experiments demonstrates that the one-pot confined growth developed herein provides a suitable strategy for the preparation of stable dispersions of metallic nanoparticles embedded into inorganic matrices through a one-pot method, giving rise to a vast plethora of composites. The optimization of the alkalization conditions allows the consolidation of a composite containing “naked” nanoparticles that is promising, for example, for catalytic applications.^[55]

Conclusion

A new methodology to obtain AuNP on the basis of homogeneous alkalization through the epoxide route was presented. The proposed method takes advantage of the controlled and simultaneous generation of OH^- and polyol moieties in the reaction medium, until a pH is reached at which Au^{III} is quantitatively reduced in the form of pure spheroidal AuNP. A stabilizing agent is required to maintain the AuNP suspension, the presence of which dramatically affects the mechanism of growth. This results in changes in the final particle shape and size, as demonstrated by the evolution of UV/Vis absorption spectra, pH, and SAXS patterns. Interestingly, the proposed methodology offers a convenient scenario to follow the reductive species concentration during the reaction (pH evolution), a feature that is not easily achievable with literature methods.

This opens up the possibility for fundamental studies concerning AuNP nucleation and growth under several conditions, and also other metal nanoparticles such as palladium or platinum, among others.

Beyond the inherent kinetic and mechanistic aspects previously discussed, the present synthesis path has certain advantages over other well-established methods. The proposed homogeneous methodology is compatible with the preparation of a wide variety of oxides and hydroxides phases that effectively stabilize the growing AuNP; these systems are also accessible to implement a comprehensive in situ inspection with the aforementioned techniques.

The inherently mild conditions employed allow the addition of thermally labile molecules, opening up the possibility of obtaining key functional materials, ranging from nanocomposites to biocapped AuNP, in a single one-pot approach.

Experimental Section

Chemicals

Gold(III) chloride trihydrate ($\text{HAuCl}_4 \cdot 3\text{H}_2\text{O}$), aluminium(III) chloride hexahydrate ($\text{AlCl}_3 \cdot 6\text{H}_2\text{O}$), hydrochloric acid (HCl), potassium chloride (KCl), polyvinylpyrrolidone $M_w = 10\,000 \text{ g mol}^{-1}$ (PVP-10k), cetyltrimethylammonium chloride (CTAC), glycerol, and glycidol (Gly) were supplied by Sigma-Aldrich. All reagents were used without further purification. Deionized water ($18 \text{ M}\Omega \text{ cm}^{-1}$) was used for all preparations.

AuNP synthesis

Typically, AuNP reduction was performed at 25°C . Experiments were carried out by mixing the filtrated solution in Milli-Q® water adjusted at a pH value of 3.0 ± 0.1 with HCl. In all cases the initial concentrations were adjusted to: $[\text{HAuCl}_4] = 0.5 \text{ mM}$, $[\text{KCl}] = 100 \text{ mM}$, $[\text{PVP-10k}] = 0.11 \text{ mM}$ or $[\text{CTAC}] = 10 \text{ mM}$, and $[\text{Gly}] = 250\text{--}5000 \text{ mM}$. Firstly, HAuCl_4 , KCl, and HCl pH 3.0 solutions were mixed; then stabilizing agent was added under continuous magnetic stirring. Au^{III} -CTAC complex formation is denoted by the formation of a bright yellow solid. In this last case, it is necessary to wait a few minutes until the opalescent mixture becomes a clear solution.

AuNP growth kinetics

Representative alkalization curves were registered by in situ potentiometric pH measurement in a reactor at 25°C under permanent magnetic stirring. The UV/Vis spectra were recorded with a Shimadzu spectrophotometer set in kinetic mode. Step time was optimized from 0.5 s/spectra to 600 s/spectra, depending on the experiment.

$\text{Al}(\text{OH})_3$ hydrogel–AuNP synthesis

A set of glycerol/water solutions (50% in volume) containing $[\text{AlCl}_3] = 500 \text{ mM}$, $[\text{Gly}] = 4400 \text{ mM}$ and variable amounts of $[\text{HAuCl}_4]$ (0, 0.25, 0.50, or 1.0 mM) were aged at 25°C for 1000 min. Absorbance values recorded at 315 and 400 nm were used to follow the overall consumption of $\text{Au}(\text{OH})_x\text{Cl}_{4-x}^-$ complexes and AuNP formation, respectively. Conductivity and proton activity were recorded along the whole gelation process by employing the proper conductimetric and potentiometric probes.

AuNP TEM inspection

As prepared AuNP suspensions were centrifuged at 11 000 RPM for 15 min and resuspended in water 2 times. These AuNP samples (15 microliters) were dropped onto a carbon-coated copper grid and left to dry. TEM inspection was performed with a Philips CM200 TEM operating at 180 kV (GM-CAC-CNEA) or a Philips EM 301 TEM operating at 60 kV (CMA, FCEN, UBA). Average sizes and size distribution of the samples were determined by counting at least 100 particles employing ImageJ software.

AuNP SAXS measurements

The SAXS measurements were performed at the D02A-SAXS1 beamline of the LNLS (Campinas, Brazil) with a wavelength of 1.544 Å. A Pilatus 300 K detector was used, with 898.39 mm sample-to-detector distance. SAXS patterns were recorded with exposure times of 20 s with 40 s of deadtime between measurements. The scattering intensity distributions as a function of scattering momentum transfer q were obtained in the q range between 0.128 and 5.9 nm^{-1} . One-dimensional curves were obtained by integration of the 2D data by employing the program FIT-2D.^[56] Measurements were performed at room temperature in a beamline vacuum-tight temperature-controlled X-ray cell for liquids.^[57] The SAXS normalized patterns were fitted by employing an in-house written program; the model's parameters were obtained for all patterns by mixing random Gaussian perturbation of the nonlinear parameters with least-square procedure in order to avoid local minima.^[58] More details can be found in the Supporting Information.

Acknowledgements

This work was supported by the University of Buenos Aires (UBA-CyT 20020130100610BA), the Agencia Nacional de Promoción Científica y Tecnológica (PICT 2015-0351, 2015-3526, 2017-4651 and 2017-3150), the National Research Council of Argentina (CONICET PIP 11220110101020) and the LNLS (proposal 20170163). Gonzalo Zbihlei is gratefully acknowledged for his help with TEM measurements. V.O. is member of ALN.

Conflict of interest

The authors declare no conflict of interest.

Keywords: gold · epoxides · kinetics · nanoparticles · sol-gel processes

- [1] M. Sanchez Dominguez, C. Rodriguez Abreu, *Nanocolloids—A Meeting Point for Scientists and Technologists*, Elsevier, Amsterdam, 2016.
- [2] P. Zhao, N. Li, D. Astruc, *Coord. Chem. Rev.* **2013**, *257*, 638.
- [3] Y. Xia, K. D. Gilroy, H.-C. Peng, X. Xia, *Angew. Chem. Int. Ed.* **2017**, *56*, 60–95; *Angew. Chem.* **2017**, *129*, 60–98.
- [4] E. Carbó-Argibay, B. Rodríguez-González, *Isr. J. Chem.* **2016**, *56*, 214–226.
- [5] B. Sepúlveda, P. C. Angelomé, L. M. Lechuga, L. M. Liz-Marzán, *Nano Today* **2009**, *4*, 244–251.
- [6] X. Ma, S. He, B. Qiu, F. Luo, L. Guo, Z. Lin, *ACS Sens.* **2019**, *4*, 782–791.
- [7] M. J. Banholzer, J. E. Millstone, L. Qin, C. A. Mirkin, *Chem. Soc. Rev.* **2008**, *37*, 885–897.
- [8] M. Fan, G. F. S. Andrade, A. G. Brolo, *Anal. Chim. Acta* **2011**, *693*, 7–25.
- [9] Y. Dai, Y. Wang, B. Liu, Y. Yang, *Small* **2015**, *11*, 268–289.
- [10] M. Stratakis, H. Garcia, *Chem. Rev.* **2012**, *112*, 4469–4506.

- [11] Y. Zhang, X. Cui, F. Shi, Y. Deng, *Chem. Rev.* **2012**, *112*, 2467–2505.
- [12] L. Liu, A. Corma, *Chem. Rev.* **2018**, *118*, 4981–5079.
- [13] E. C. Dreaden, A. M. Alkilany, X. Huang, C. J. Murphy, M. A. El-Sayed, *Chem. Soc. Rev.* **2012**, *41*, 2740–2779.
- [14] C. M. Cobley, J. Chen, E. C. Cho, L. V. Wang, Y. Xia, *Chem. Soc. Rev.* **2011**, *40*, 44–56.
- [15] R. A. Sperling, P. Rivera Gil, F. Zhang, M. Zanella, W. J. Parak, *Chem. Soc. Rev.* **2008**, *37*, 1896–1908.
- [16] P. D. Howes, S. Rana, M. M. Stevens, *Chem. Soc. Rev.* **2014**, *43*, 3835–3853.
- [17] D. García-Lojo, S. Núñez-Sánchez, S. Gómez-Graña, M. Grzelczak, I. Pastoriza-Santos, J. Pérez-Juste, L. M. Liz-Marzán, *Acc. Chem. Res.* **2019**, *52*, 1855–1864.
- [18] P. C. Angelomé, L. M. Liz-Marzán, *J. Sol-Gel Sci. Technol.* **2014**, *70*, 180–190.
- [19] P. Innocenzi, L. Malfatti, *J. Nanopart. Res.* **2018**, *20*, 167.
- [20] J. Turkevich, P. C. Stevenson, J. Hillier, *Discuss. Faraday Soc.* **1951**, *11*, 55.
- [21] G. Frens, *Nat. Phys. Sci.* **1973**, *241*, 20–22.
- [22] K. Zabetakis, W. E. Ghann, S. Kumar, M. C. Daniel, *Gold Bull.* **2012**, *45*, 203–211.
- [23] I. Ojea-Jiménez, N. G. Bastús, V. Puentes, *J. Phys. Chem. C* **2011**, *115*, 15752–15757.
- [24] F. Schulz, T. Homolka, N. G. Bastús, V. Puentes, H. Weller, T. Vossmeier, *Langmuir* **2014**, *30*, 10779–10784.
- [25] F. Kettmann, A. Birnbaum, S. Witte, M. Wuthschick, N. Pinna, R. Kraehnert, K. Rademann, J. Polte, *Chem. Mater.* **2016**, *28*, 4072–4081.
- [26] E. B. Ferreira, J. F. Gomes, G. Tremiliosi-Filho, L. H. S. Gasparotto, *Mater. Res. Bull.* **2014**, *55*, 131–136.
- [27] R. Parveen, G. Tremiliosi-Filho, *RSC Adv.* **2016**, *6*, 95210–95219.
- [28] J. F. Gomes, A. C. Garcia, E. B. Ferreira, C. Pires, V. L. Oliveira, G. Tremiliosi-Filho, L. H. S. Gasparotto, *Phys. Chem. Chem. Phys.* **2015**, *17*, 21683–21693.
- [29] R. Parveen, S. Ullah, R. Sgarbi, G. Tremiliosi-Filho, *Coll. Surfaces A: Physicochem. Eng. Aspects* **2019**, *565*, 162–171.
- [30] R. Parveen, J. F. Gomes, S. Ullah, J. J. S. Acuña, G. Tremiliosi-Filho, *J. Nanopart. Res.* **2015**, *17*, 418.
- [31] T. S. Rodrigues, M. Zhao, T.-H. Yang, K. D. Gilroy, A. G. M. da Silva, P. H. C. Camargo, Y. Xia, *Chem. Eur. J.* **2018**, *24*, 16944–16963.
- [32] V. Oestreicher, M. Jobbágy, *Langmuir* **2013**, *29*, 12104–12109.
- [33] N. Tarutani, Y. Tokudome, M. Jobbágy, F. A. Viva, G. J. A. A. Soler-Illia, M. Takahashi, *Chem. Mater.* **2016**, *28*, 5606–5610.
- [34] Y. Tokudome, M. Fukui, N. Tarutani, S. Nishimura, V. Prevot, C. Forano, G. Poologasundarampillai, P. D. Lee, M. Takahashi, *Langmuir* **2016**, *32*, 8826–8833.
- [35] A. E. Gash, T. M. Tillotson, J. H. Satcher, L. W. Hrubesh, R. L. Simpson, *J. Non-Cryst. Solids* **2001**, *285*, 22–28.
- [36] N. Arencibia, V. Oestreicher, F. A. Viva, M. Jobbágy, *RSC Adv.* **2017**, *7*, 5595–5600.
- [37] V. Oestreicher, D. Hunt, R. Torres-Cavanillas, G. Abellán, D. A. Scherlis, M. Jobbágy, *Inorg. Chem.* **2019**, *58*, 9414–9424.
- [38] V. Oestreicher, I. Fábregas, M. Jobbágy, *J. Phys. Chem. C* **2014**, *118*, 30274–30281.
- [39] Y. Tokudome, T. Morimoto, N. Tarutani, P. D. Vaz, C. D. Nunes, V. Prevot, G. B. G. Stenning, M. Takahashi, *ACS Nano* **2016**, *10*, 5550–5559.
- [40] T. M. Tillotson, W. E. Sunderland, I. M. Thomas, L. W. Hrubesh, *J. Sol-Gel Sci. Technol.* **1994**, *1*, 241–249.
- [41] Y. Tokudome, A. Miyasaka, K. Nakanishi, T. Hanada, *J. Sol-Gel Sci. Technol.* **2011**, *57*, 269–278.
- [42] V. Oestreicher, M. Jobbágy, *Chem. Commun.* **2017**, *53*, 3466–3468.
- [43] T. Hendel, M. Wuthschick, F. Kettmann, A. Birnbaum, K. Rademann, J. Polte, *Anal. Chem.* **2014**, *86*, 11115–11124.
- [44] J. A. Peck, C. D. Tait, B. I. Swanson, G. E. Brown, *Geochim. Cosmochim. Acta* **1991**, *55*, 671–676.
- [45] C. Noguez, *J. Phys. Chem. C* **2007**, *111*, 3806–3819.
- [46] A. Usher, D. C. McPhail, J. Brugger, *Geochim. Cosmochim. Acta* **2009**, *73*, 3359–3380.
- [47] J. Rodríguez-Fernández, J. Pérez-Juste, P. Mulvaney, L. M. Liz-Marzán, *J. Phys. Chem. B* **2005**, *109*, 14257–14261.
- [48] F. Pschunder, J. Puig, L. J. Giovanetti, C. Huck-Iriart, F. G. Requejo, D. Buceta, C. E. Hoppe, J. M. Ramallo-López, *J. Phys. Chem. C* **2018**, *122*, 29051–29061.
- [49] N. Tarutani, Y. Tokudome, M. Jobbágy, G. J. A. A. Soler-Illia, Q. Tang, M. Müller, M. Takahashi, *Chem. Mater.* **2019**, *31*, 322–330.
- [50] J. S. Pedersen, *Adv. Colloid Interface Sci.* **1997**, *70*, 171–210.
- [51] B. H. Zimm, *J. Chem. Phys.* **1948**, *16*, 1093–1099.
- [52] C. Huck-Iriart, J. Montes-de-Oca-Ávalos, M. L. Herrera, R. J. Candal, C. L. Pinto-de-Oliveira, I. Linares-Torriani, *Food Res. Int.* **2016**, *89*, 338–346.
- [53] V. Oestreicher, M. Perullini, M. Jobbágy, *Dalton Trans.* **2016**, *45*, 9920–9924.
- [54] Y. Tokudome, K. Nakanishi, K. Kanamori, T. Hanada, *J. Colloid Interface Sci.* **2010**, *352*, 303–308.
- [55] N. G. Bastús, F. Merkoçi, J. Piella, V. Puentes, *Chem. Mater.* **2014**, *26*, 2836–2846.
- [56] A. Hammersley, *J. Appl. Crystallogr.* **2016**, *49*, 646–652.
- [57] L. P. Cavalcanti, I. L. Torriani, T. S. Plielic, C. L. P. Oliveira, G. Kellermann, R. Neuenschwander, *Rev. Sci. Instr.* **2004**, *75*, 4541–4546.
- [58] D. da Silva Costa, C. Huck-Iriart, G. Kellermann, L. J. Giovanetti, A. F. Craievich, F. G. Requejo, *Appl. Phys. Lett.* **2015**, *107*, 223101.

 Manuscript received: November 25, 2019

Revised manuscript received: December 28, 2019

Accepted manuscript online: January 9, 2020


Version of record online: ■■■■■ 0000

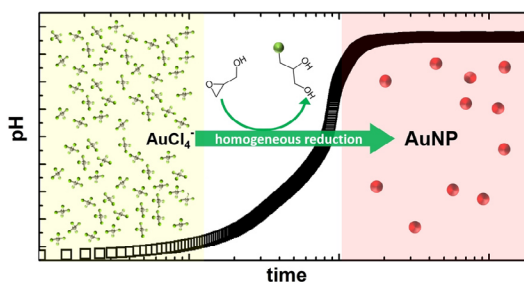
FULL PAPER

Gold

V. Oestreicher,* C. Huck-Iriart,
G. Soler-Illia, P. C. Angelomé, M. Jobbágy*



 Mild Homogeneous Synthesis of Gold Nanoparticles through the Epoxide Route: Kinetics, Mechanisms, and Related One-Pot Composites



Homogeneous alkalization leads to the quantitative formation of gold nanoparticles at room temperature by means of epoxide ring-opening. The new methodology takes advantage of the kinetically controlled generation of

OH^- in the reaction medium; under alkaline conditions spheroidal Au nanoparticles are formed. The required stabilizing agents affect the mechanism of growth and kinetics, as demonstrated by spectroscopic measurements.